Colloquia: SIRR 2020

Theoretical study for a ^{117m}Sn production experiment with a 30 MeV α-beam cyclotron

F. Barbaro[1][2][*], L. De Dominicis[3][4], L. Canton[1], M. P. Carante[5], A. Colombi[2][5], A. Fontana[5] and A. Stolarz[4]

[1] *INFN, Sezione di Padova - Padova, Italy*
[2] *Dipartimento di Fisica, Università di Pavia - Pavia, Italy*
[3] *Dipartimento di Fisica, Università di Padova - Padova, Italy*
[4] *Heavy Ion Laboratory, University of Warsaw - Warsaw, Poland*
[5] *INFN, Sezione di Pavia - Pavia, Italy*

Summary. — Metastable ^{117m}Sn is a promising theranostic radionuclide, suitable for SPECT diagnostic imaging and conversion electron therapy. Its production is based mainly on nuclear reactors, but there is increasing interest in alternative routes with cyclotrons. Theoretical studies are essential to identify the irradiation parameters and conditions to maximize its production, while minimizing the impact of the contaminants. The goal of this study is to investigate the production of ^{117m}Sn with a 30 MeV α beam on ^{nat}Cd and ^{nat}In targets, as provided by the HIL-UW (Heavy Ion Laboratory - University of Warsaw) U-200P cyclotron. We performed a theoretical analysis of cross section, yield and purity by means of two nuclear reaction codes: Talys (v.1.9), based on a combination of models, and Fluka (v.2018.2.dev), based on Monte Carlo simulations. We compared the theoretical calculations with both experimental data already known in the literature and preliminary results obtained at HIL. A statistical treatment of the models suggests a comparable production of ^{117m}Sn for both targets, but a higher radionuclidic purity was found in the case of the ^{nat}In target.

1. – Introduction

Nowadays ^{117m}Sn ($T_{1/2} = 13.76$ d) is mainly produced by nuclear reactors with low specific activity. Cyclotrons represent a new route to be investigated to obtain an efficient production, possibly with a high radionuclidic purity [1]. The interest on ^{117m}Sn is based

---

[*] Corresponding author. E-mail: francesca.barbaro@pd.infn.it

on its nuclear features suitable for theranostic applications, *i.e.*, appropriate both for diagnosis and therapy. Its γ-emission, with energy and branching ratio given by $E = 156.02$ (2.113%) and 158.56 (86.4%) keV, is compatible with a SPECT diagnostic imaging application. Furthermore, as conversion electrons emitter, with $E = 126.82$ (65.7%), 129.360 (11.65%), and 151.56 (26.5%) keV, it is suitable for the treatment and palliative care of bone metastases, entailing the delivery of a high dose of radiation within the metastasis sites and a relative sparing of the bone marrow. At present ^{117m}Sn is not used in medical practice, although a variety of chelators has been already developed and tested and research is ongoing in pre-clinical and clinical trials. For example, ^{117m}Sn(4+)DTPA [2] is found to be a good agent to treat bone disease, suitable also for effective pain relief with no significant myelotoxicity. ^{117m}Sn, chelated to aminobenzyl-DOTA and conjugated to annexin V-128, was applied for imaging and treatment of atherosclerotic vulnerable plaques (VP), and recent studies demonstrate the selective uptake of the Sn-annexin in cardiovascular VP, identifying this agent with high specific activity as a suitable inflammatory tracer for cardiovascular disease [3, 4]. This application underlines the need for high specific activity which is likely to be obtained with accelerators rather than nuclear reactors [5]. Moreover, the study confirms that ^{117m}Sn γ decay is suitable for diagnostic imaging and its conversion electron emission provides a therapeutic effect to inflammatory tissue when used in doses typical for imaging studies. New research on the use of high specific activity ^{117m}Sn for treating immunity, inflammation and degenerative joints are ongoing. Radionuclide synovectomy (RS) is a minimally invasive method in which the injection of a radionuclide in colloidal form into the synovial membrane of diseased joints aims at treating rheumatoid arthritis, hemophilia arthritis and osteoarthritis. The long-term effects of this treatment are comparable to arthroscopic or open synovectomy, with the advantage of no surgery side effects and no need of rehabilitation. The interest on ^{117m}Sn applied to RS depends on its emission of conversion electrons that are responsible for a strong dose delivery in a limited range (around $300\,\mu$m), minimizing the collateral damage of the surrounding tissues [6]. On the basis of these references, further studies to investigate the production of ^{117m}Sn with cyclotrons are needed and our work concerns with this aim.

2. – Methods

To support the experimental investigations ongoing at U-200P cyclotron (HIL) we performed a theoretical analysis of the production of ^{117m}Sn considering a 30 MeV α-beam impinging on ^{nat}Cd and ^{nat}In targets [7]. We considered the two nuclear reaction codes `Fluka` [8] and `Talys` [9]. `Fluka` is a general purpose Monte Carlo code for modelling particle transport and interactions with matter. Radionuclide production is described by the intranuclear cascade model which is based on the PEANUT (PreEquilibrium Approach to Nuclear Thermalisation) module and the code for each reaction channel returns the cross sections directly from the probability of creating the specific nuclide in a collision. `Talys`, instead, provides several pre-equilibrium (PE) and level-density (LD) models. The description of the PE processes is based on the exciton model, in which a nuclear state is defined by the number of excitons and by the corresponding excitation energy. Transition matrices are the basic building blocks of this formalism and they are described analytically (PE 1), numerically (PE 2) or obtained with the imaginary component of the optical potential (PE 3). There is also a PE 4 option, but we did not consider it because we found some problems of stability in the evaluation of these cross sections. The Hauser-Feshbach formalism for the compound nucleus formation implies an

energy averaging of the transmission coefficients over the residual-nucleus level densities. Talys considers three phenomenological LD models, namely the Fermi gas with constant temperature (LD 1), the back-shifted Fermi gas (LD 2), and the generalised superfluid model (LD 3) and three microscopic models, that is the Goriely's tabulated Hartree-Fock densities (LD 4), the Hilaire's tabulation based upon the combinatorial model (LD 5), and the Hartree-Fock-Bogoliubov temperature-dependent formalism (LD 6). This leads to a total of 18 cross sections based upon the combination of 3×6 different models. The variability of these models has been investigated by a statistical dispersion analysis which provides an interquartile range, measuring the dispersion between the lower Q1 and the upper Q3 quartile. Furthermore we introduced as reference calculation the centre of the interquartile band, denoted as best theoretical evaluation (BTE) [10]. The Talys "default" calculation (identified with PE 2 and LD 1) and the min/max limits spanned by all the 18 combinations of models have also been added in the analysis.

In the first place we calculate, with the reaction codes, the production cross sections $\sigma_i(E)$ for a given radionuclide i. From these the production rate R_i [11] is evaluated with the equation

$$(1) \qquad R_i = \frac{I_0 N_a}{z_{proj} e A} \int_{E_{out}}^{E_{in}} \sigma_i(E) \left(\frac{\mathrm{d}E}{\rho_t \mathrm{d}x} \right)^{-1} \mathrm{d}E,$$

where I_0 is the beam current, N_a the Avogadro number, z_{proj} the atomic number of the incident particle, e the electron charge, A the target atomic mass, ρ_t the target density, E_{in} and E_{out} the energy of the projectile impinging on the target and leaving the target, respectively. The stopping power $\mathrm{d}E/\mathrm{d}x$ of the projectile in the target has been calculated with the Bethe-Bloch formula [12].

We solved numerically the generalized Bateman equation that describes the radioactive decay chain by a system of ordinary differential equations,

$$(2) \qquad \frac{\mathrm{d}N_i(t)}{\mathrm{d}t} = R_i - \lambda_i N_i(t) + \sum_{j<i} f_{ij} \lambda_j N_j(t),$$

where $N_i(t)$ is the number of nuclei of species i produced at time t, λ_i the decay constant, and f_{ij} the branching ratio from j to i.

Nevertheless the nuclear reaction $^{nat}Cd(\alpha, x)^{117m}$Sn is a complex case where the interplay of ^{117g,m}Sn involves also the intermediate products ^{117g,m}In, since they decay into ^{117m}Sn, as well. Consequently, we enlarged the system of coupled differential equations to take into account also the decay of this two intermediate nuclides.

The solution of the differential equations provides the time evolution of $N_i(t)$, that is the number of nuclei of the species i. Finally we introduce the activity produced at the irradiation time t,

$$(3) \qquad A_i(t) = \lambda_i N_i(t),$$

and the integral yield at the end of bombardment (EOB),

$$(4) \qquad y_{i\,EOB} = A_i(T)/I_0,$$

where T is the time at EOB and I_0 is the above-defined beam current.

Measurements of the ^{117m}Sn cross sections have been performed at the U-200P cyclotron at HIL. The internal configuration for the new target station was exploited to irradiate with a 30 MeV α-beam two different stacked-foil targets: one containing two ^{nat}Cd foils and the other containing the ^{nat}In ones. These foils were, in both cases, alternated to ^{nat}Al degrader foils, to degrade the beam energy, and ^{nat}Ti and ^{nat}Cu monitor foils, to control the beam flux across the target. The target structure allowed to obtain more than one cross section value, corresponding to different energies, in one single irradiation run. After the EOB the target was disassembled and each foil was measured several times with a CANBERRA HPGe detector. The first measurements occurred immediately after the EOB to acquire also the short-lived radionuclides in the γ spectra. Further measurements were then performed at given time intervals to follow the decay processes. Late γ acquisitions allow to have the ^{117m}Sn 158 keV γ peak without the interference of shorter-lived ^{117}In and, in the case of ^{nat}In targets, also of ^{117}Sb. From the γ spectra one derives the cross sections and uncertainties following the formulas by Otuka *et al.* [13]. The results obtained from each γ acquisition of the same foil were combined in a weighted average to have the final value. The beam-energy loss inside the target, derived from a simulation with SRIM-2013 [14], was taken into account.

3. – Results

We analysed cross sections and yields for ^{117m}Sn and its main contaminants ^{113g}Sn ($T_{1/2} = 115.09$ d) and ^{119m}Sn ($T_{1/2} = 293.1$ d), and for both targets. Model calculations have been compared to the preliminary results obtained at HIL and to previous data obtained from EXFOR database [15-23].

In fig. 1 the low-energy peak is better reproduced by `Talys` than by `Fluka`: a possible explanation could originate from a different treatment of the low energy range, specifically below 30 MeV. The HIL preliminary results are consistent with the other data, however, additional experimental data around 15 MeV could be important to confirm the position
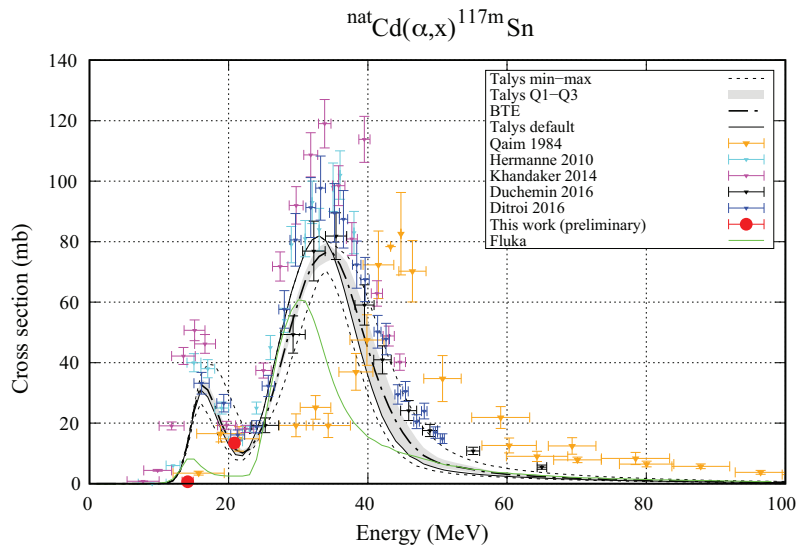

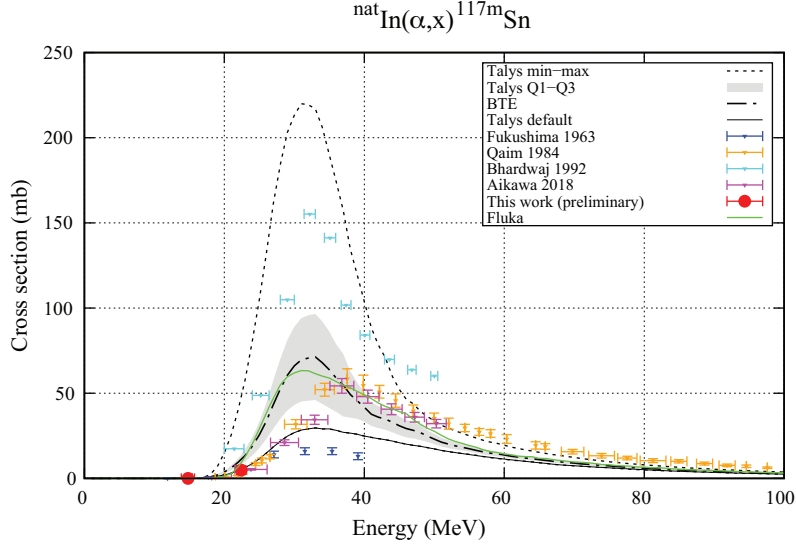Fig. 1. – Cross section for ^{nat}Cd$(\alpha, x)^{117m}$Sn.

Fig. 2. – Cross section for $^{nat}\mathrm{In}(\alpha, x)^{117m}\mathrm{Sn}$.

and intensity of the first peak. It is evident that for the $^{nat}\mathrm{Cd}(\alpha, x)^{117m}\mathrm{Sn}$ reaction the interquartile band is significantly narrow indicating that the range of variability of all `Talys` models is rather limited. On the contrary, the spread of experimental data demands more accurate measurements to compare with model calculations. A larger variability of `Talys`-model calculations is shown in fig. 2 for the $^{nat}\mathrm{In}(\alpha, x)^{117m}\mathrm{Sn}$ cross section. Moreover, both `Talys` and `Fluka` anticipate the position of the peak described by the data. Similarly to the previous figure also here there is a significant spread of experimental data, suggesting the need for new measurements such as those ongoing and planned at HIL.

It is important to evaluate also the production of contaminants as shown in figs. 3 and 4 for $^{nat}\mathrm{Cd}$ and $^{nat}\mathrm{In}$, respectively, where all curves refer to `Talys` default. In fig. 3 there is an evident dominance of the $^{113m}\mathrm{Sn}$ cross section overwhelming the $^{117m}\mathrm{Sn}$ production. In the intermediate energy range, above 30 MeV, also $^{111}\mathrm{Sn}$ outperforms the $^{117m}\mathrm{Sn}$ cross section, while at energies above 45 MeV a third radionuclide, $^{110}\mathrm{Sn}$, is also produced more abundantly. Their half-lives are much smaller than the 13.76 days of $^{117m}\mathrm{Sn}$ and this is particularly true at low energies with $^{113m}\mathrm{Sn}$ and $^{111}\mathrm{Sn}$ half-lives of 21.4 and 35.3 minutes, respectively. Unfortunately, $^{113m}\mathrm{Sn}$ decays with branching ratio of 91.10% into $^{113g}\mathrm{Sn}$ with an half-life of 115.09 days. This makes the $^{nat}\mathrm{Cd}$ target a production route with low purity. On the contrary, in fig. 4 no contaminants overlap occurs in the energy region corresponding to the peak of $^{117m}\mathrm{Sn}$ cross section, suggesting that this reaction could be a good candidate for high-purity production. In order to analyse the quality of the yields we identified two optimal irradiation energy windows in the range 20–40 MeV and 25–35 MeV for $^{nat}\mathrm{Cd}$ and $^{nat}\mathrm{In}$, respectively.

First we calculate the integral yields for a current $I_0 = 1\,\mu\mathrm{A}$ and $T = 24\,\mathrm{h}$ at EOB, whose irradiation energy range is set from E_{max} to 0, namely, assuming full beam energy loss inside the target. The results are plotted in figs. 5 and 6 using the BTE (solid line), the interquartile range (gray area), and the min/max of the 18 combinations of `Talys` models (thin dashed lines). From the integral yields shown in these figures we obtained
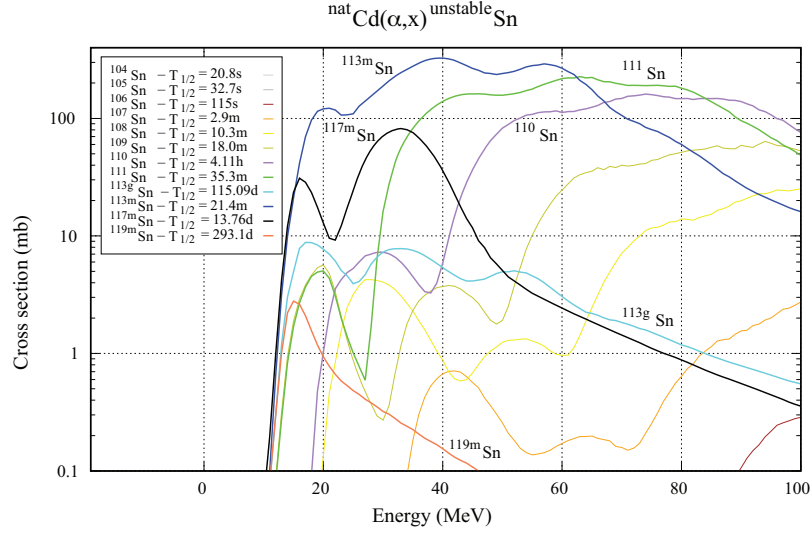
Fig. 3. – `Talys` default cross sections of ^{117m}Sn and main contaminants in the case of the ^{nat}Cd target.

the yield for the two specific irradiation energy windows by selecting the corresponding energies E_{in} and E_{out} within the green area. The yield for a target of selected thickness is simply given by the difference $y_{i\,EOB}(E_{in}) - y_{i\,EOB}(E_{out})$.

In table I, we report the resulting yields for ^{117m}Sn and its contaminants, where we impose the additional restriction of E_{in} to 32 MeV, in line with the maximum beam energy available at HIL. The yield values with the selected irradiation conditions correspond to a target thickness of 110 and 85 μm for ^{nat}Cd and ^{nat}In, respectively. The table shows
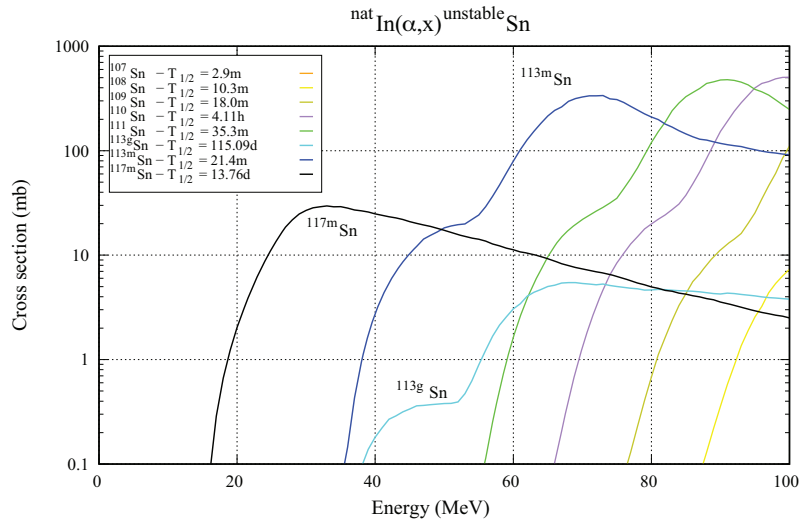

Fig. 4. – `Talys` default cross sections of ^{117m}Sn and main contaminants in the case of the ^{nat}In target.

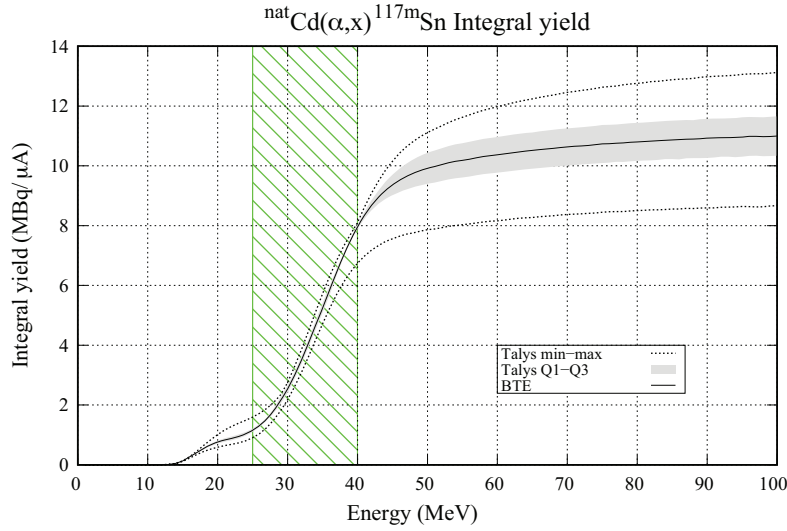Fig. 5. – Integral yield of ^{117m}Sn in the case of the ^{nat}Cd target.

that the ^{117m}Sn production from the two targets is comparable, however in the case of ^{nat}In there is a much larger model dependence. Moreover the table clearly confirms what we already derived in discussing the figures: the reaction with ^{nat}In is much less affected by contaminant production than the one with ^{nat}Cd and should therefore be considered more promising.

In addition, to complete the theoretical analysis, we have also investigated the effect of the intermediate ^{117g,m}In production in the reaction with both ^{nat}Cd and ^{nat}In targets. In the first case our findings indicate an additional 5% increase of the ^{117g}Sn production (99.83% branching ratio) and a negligible enhancement for ^{117m}Sn (0.17% branching

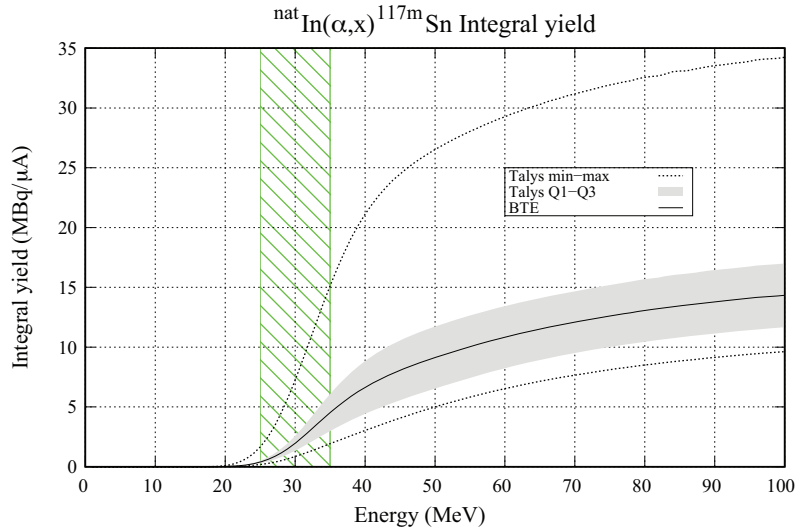Fig. 6. – Integral yield of ^{117m}Sn in the case of the ^{nat}In target.

TABLE I. – *Predicted yields for ^{117m}Sn and main contaminants, for both ^{nat}Cd and ^{nat}In targets.*

24 h irradiation	Yield (MBq/μA)	
	^{nat}Cd (32–20 MeV)	^{nat}In (32–25 MeV)
^{117m}Sn	2.75 $\pm$ 0.21	2.56 $\pm$ 1.09
^{113g}Sn	1.16 $\pm$ 0.07	1.0E-05 $\pm$ 8.0E-07
^{119m}Sn	2.2E-03 $\pm$ 5.0E-04	–

ratio) due to ^{117g}In decay. For the second target, the cross sections for both ^{117g}In and ^{117m}In are very low, below 0.1 and 0.025 mb, respectively, and they do not contribute significantly to the ^{117m}Sn production.

4. – Conclusions

We have investigated the production of theranostic ^{117m}Sn considering an α-beam with energies up to 32 MeV impinging on ^{nat}Cd and ^{nat}In targets. Nuclear reaction model calculations have been performed with `Talys` and `Fluka` codes. Within the `Talys` code, the production of the radionuclide has been described using a statistical treatment of the models variability. As a result of this study we found that the production yield of ^{117m}Sn for both targets are comparable for similar irradiation conditions. However, for the ^{nat}Cd$(\alpha, x)^{117m}$Sn reaction the resulting interquartile band is significantly narrow, while for the ^{nat}In$(\alpha, x)^{117m}$Sn case the band is much wider, indicating a more pronounced model dependence, which points to the need for new accurate data. On the other hand, if we look at the available experimental measurements we observe a significant spread of the data, which restates the need for new, accurate data for the relevant cross sections. Preliminary new data on both targets obtained at HIL-UW are reported in this work.

Also the impact of the contaminants on the production quality has been investigated. The main focus is on ^{113g}Sn and ^{119m}Sn, because their half-lives are longer than that of ^{117m}Sn and they cannot be eliminated by the time evolution of the product. In addition, the production of ^{113m}Sn, with an half-life of 21.4 minutes, has an important impact because it decays into ^{113g}Sn with a branching ratio of 91.10%, specifically with ^{nat}Cd, where the cross section is quite large. The findings indicate that both targets can be utilized for a significant and comparable production of the radionuclide ^{117m}Sn, but the ^{nat}In appears to be more promising for a production with a high radionuclidic purity, due to the absence of ^{119m}Sn contamination and a much lower ^{113m}Sn cross section in the considered energy range.

* * *

REFERENCES

[1] Vučina J. *et al.*, *Proceedings of the 5th Yugoslav Nuclear Society Conference, Belgrade, Serbia and Montenegro*, edited by Antic D. (Institut za Nuklearne Nauke VINCA, Belgrade, Serbia) 2005, pp. 325–328.
[2] Bishayee A. *et al.*, *J. Nucl. Med.*, **41** (2000) 2043.
[3] Stevenson N. R. *et al.*, in *International Conference on Integrated Medical Imaging in Cardiovascular Diseases* (IAEA, 2013) IAEA-CN-202/254.
[4] Jaimovich R. *et al.*, in *International Conference on Integrated Medical Imaging in Cardiovascular Diseases* (IAEA, 2013) IAEA-CN-202/212.
[5] Stevenson N. R. *et al.*, *J. Radioanal. Nucl. Chem.*, **305** (2015) 99.
[6] Srivastava S. C., *Braz. Arch. Biol. Technol.*, **50** (2007) 49.
[7] Barbaro F. *et al.*, LNL Annual Report 2019, INFN-LNL Report 259 (2020), ISSN 1828-8561.
[8] Battistoni G. *et al.*, *AIP Conf. Proc.*, **896** (2006) 31.
[9] Goriely S., Hilaire S. and Koning A. J., *Astron. Astrophys.*, **487** (2008) 767.
[10] Carante M. P. *et al.*, LNL Annual Report 2019, INFN-LNL Report 259 (2020), ISSN 1828-8561.
[11] Canton L. and Fontana A., *Eur. Phys. J. Plus*, **135** (2020) 770.
[12] Leo W. R., *Techniques for Nuclear and Particle Physics Experiments* (Springer) 1994.
[13] Otuka N. *et al.*, *Radiat. Phys. Chem.*, **140** (2017) 502.
[14] Ziegler J. F. *et al.*, *Nucl. Instrum. Methods Phys. Res. B*, **268** (2010) 1818.
[15] EXFOR database, https://www-nds.iaea.org/exfor/exfor.html.
[16] Qaim S. M. and Döhler H., *Int. J. Appl. Radiat. Isotopes*, **35** (1984) 645.
[17] Hermanne A. *et al.*, *Nucl. Instrum. Methods Phys. Res. B*, **268** (2010) 1376.
[18] Khandaker M. U. *et al.*, *Nucl. Instrum. Methods Phys. Res. B*, **333** (2014) 80.
[19] Duchemin C. *et al.*, *Appl. Radiat. Isotopes*, **115** (2016) 113.
[20] Ditrói F. *et al.*, *Appl. Radiat. Isotopes*, **118** (2016) 266.
[21] Fukushima S. *et al.*, *Bull. Chem. Soc. Jpn*, **36** (1963) 1225.
[22] Bhardwaj M. K. *et al.*, *Int. J. Mod. Phys. E*, **01** (1992) 389.
[23] Aikawa M. *et al.*, *Nucl. Instrum. Methods Phys. Res. Sect. B*, **426** (2018) 18.